Hindawi
Mathematical Problems in Engineering
Volume 2020, Article ID 9786895, 16 pages
https://doi.org/10.1155/2020/9786895

Research Article

Research on Energy-Saving Design of Rural Building Wall in Qinba Mountains Based on Uniform Radiation Field

Qin Zhao, Xiaona Fan, Qing Wang, Guochen Sang, and Yiyun Zhu

Department of Civil Engineering, Xi'an University of Technology, Xi'an 710048, China

Correspondence should be addressed to Yiyun Zhu; zhuyiyun006@126.com

Received 6 May 2020; Accepted 5 June 2020; Published 2 September 2020

Academic Editor: Yumin Cheng

How to create a healthy and comfortable indoor environment without causing a substantial increase in energy consumption has become a strategic problem that the development of all countries must face and solve. According to the climatic conditions of Qinba Mountains in China, combined with the characteristics of local rural residential buildings and residents' living habits, the field survey and theoretical analysis were used to study the thermal environment status and the heating energy consumption condition of local rural residential buildings. The thermal design method of walls for the local rural energy-saving buildings based on the indoor uniform radiation field was explored by using the outdoor comprehensive temperature function expressed by the fourth-order harmonic Fourier series as the boundary condition of the wall thermal analysis. ANSYS CFX was adopted to study the suitability of the energy-saving wall structure designed by the above method. The results show that the indoor thermal environment of local rural residential buildings in winter is not ideal and the heating energy consumption is high, but this area has the geographical advantage to develop solar energy buildings. It is proposed that the indoor thermal comfort temperature of local rural residential buildings in winter should not be lower than 14°C. When the internal surface temperature of the external walls in different orientations are equally based on the design principle of uniform radiation field, the heat transfer coefficient of the east wall, the west wall, and the north wall of the local rural residential buildings is 1.13 times, 1.06 times, and 1.14 times of the south wall heat transfer coefficient, respectively. The energy-saving structural wall with KPI porous brick as the main material and the south wall heat transfer coefficient of 0.9 W/(m^2·K) is the most suitable energy-saving wall for local rural residential buildings.

1. Introduction

Many research studies have shown that good environmental conditions can enhance people's productivity and happiness [1–4]. People spend more than 90% of their time indoors, especially for the old, the weak, the sick, and the disabled [5, 6]. Therefore, a comfortable indoor thermal environment is necessary. However, with the improvement of indoor thermal comfort, the proportion of building energy consumption is also increasing [7–9]. At present, energy consumption in buildings already accounts for nearly 40% of total energy consumption in China, a figure which is still rising [10–12]. If the rapid growth of building energy consumption cannot be controlled, the present development model will bring negative effects to the sustainable development of China's national economy, which is still the top priority of developing countries. Therefore, how to create a healthy, comfortable, and safe building indoor environment without causing a substantial increase in energy consumption has become a strategic problem that countries must face and solve.

Currently, more than 560 million people are living in China's rural areas [13], with a total building area of 24 billion m^2 [14], accounting for 50% of the total building area in China [15]. According to the projections of the World Bank, even if China maintains a stable urbanization rate, its rural population will still be more than 500 million by 2030 [16]. If the thermal design and construction of buildings are not rationalized, the energy consumption in rural residential buildings will continue to increase in the future [17–19]. Therefore, promoting and accelerating the sustainable development of rural buildings have a strategic meaning for

balancing the contradiction between building energy efficiency and indoor thermal environment improvement.

The energy-saving of the envelope is considered to be one of the most effective ways of building energy-saving [20–23]. The external wall is the main part of the building envelope [24, 25]. Among the energy consumption of the building envelope, the heat consumption of the external wall accounts for the largest proportion [26, 27]. Thus, it is an important measure to reduce building energy consumption and improve the indoor thermal environment by optimizing the thermal design and structural design of external walls. So far, many scholars have conducted research on the energy-saving structure design of the wall [28–31] and indicated that indoor thermal environment quality can be effectively improved, and building energy consumption can be significantly reduced if external walls can be rationalized in design and construction.

Generally, the heat transfer coefficient of the wall with different orientations is considered to be the constant in building thermal design [31, 32]. Nevertheless, for some areas with high solar radiation intensity, the solar radiation intensity varies greatly in different orientations [33, 34]. In the thermal design of the wall, the same heat transfer coefficient is adopted for the external walls with different orientations, which greatly simplifies the thermal design process of the wall. However, the above design method neglects the influence of solar radiation difference in different orientations on wall heat transfer and also fails to consider the economics of the wall structure and the influence of the wall thermal performance on the indoor thermal comfort [31].

The effect of the wall on the indoor thermal environment and energy consumption of the building is influenced by the thermal performance, the construction mode, and the construction materials of the wall. The walls with the same heat transfer coefficient but different construction methods or construction materials have different influences on the indoor thermal environment and building energy consumption. However, in the research of building external walls, there is a lack of research on structural optimization of energy-saving walls based on the uniform radiation field, especially the research methods of steady-state theoretical calculation and dynamic numerical simulation [31, 35–37]. Many scholars have conducted researches on rural residential buildings [38–40]. These researches show that it is important to fully consider the climate characteristics and residents' living habits in building design, which can enable buildings to be environmentally friendly, low-energy consuming, and sustainable on a longer term. Therefore, it is an important measure to reduce the building energy consumption and improve the indoor thermal environment of the rural residential buildings by reasonably controlling the thermal parameters, construction methods, and construction materials of the external walls according to the specific climatic conditions, building characteristics, and residents' living habits.

The Qinba mountains are located in the northern high latitude area of the hot summer and cold winter area, between the Qinling mountains and the Baba mountains, including three cities, Hanzhong, Ankang, and Shangluo [41, 42]. The area is hot and humid in summer and cold and wet in winter [43]. The temperature in the lowest month is similar to that in the cold area, and the minimum outdoor temperature can reach about −10°C [44, 45]. The annual sunshine hours are from 1400~2200 h, and the annual solar radiation amount is from 4190~5016 $MJ \cdot m^{-2} \cdot a^{-1}$ [46]. Consequently, the thermal effect of indoor and outdoor environment on the building envelope in this area is quite different from that of other areas with hot summer and cold winter. The amount of rural buildings in Qinba mountains area is large and widely distributed. However, the building type is simple and the structure is extensive, which contributes to the poor thermal environment indoor in winter and high heating energy consumption [43, 47]. Therefore, problems such as poor indoor thermal environment and high heating energy consumption are particularly prominent in this area.

Ankang area is located in the intersection zone of Sichuan, Chongqing, Hubei, and Shaanxi provinces, and its climate characteristics and residential forms are representative in Qinba mountains [48, 49]. According to the climate conditions of Qinba mountains, combined with the characteristics of rural residential buildings and the living habits of residents in Ankang area, the field survey and theoretical analysis were used to study the indoor and outdoor thermal environment status and the heating energy consumption condition of local rural residential buildings and explore the thermal design method of walls for the local rural energy-saving buildings based on the indoor uniform radiation field. In addition, ANSYS CFX was adopted to study the suitability of the energy-saving wall structure designed by the above method. The research results can provide theoretical and technical reference for the construction of rural residential buildings in Qinba mountains and other similar areas and play an important role in promoting the sustainable development of rural buildings.

2. Current Situation of Indoor and Outdoor Thermal Environment and Heating înergy Consumption

2.1. Object Selection. We conducted a field survey of rural residential buildings in Sanyuan Village, Ankang City, and Shaanxi Province of China from January 1 to 3, 2016.

According to the survey, it is found that most of the rural residential buildings in Qinba Mountains are two-story independent buildings with households as units. Most of the local residential buildings face south, with a long east-west and short north-south layout. The external walls are mostly 240-mm-thick solid clay brick wall. The roof is flat or in double slope. Most of the windows are in single frame and made of aluminum alloy or plastics. Based on the above analysis, a representative two-story independent residential building (Figure 1) is selected as the following measurement and analysis.

Figure 1: The south facade of representative building.

2.2. Data Acquisition. A field measurement was conducted to obtain the indoor and outdoor thermal environment parameters. The outdoor temperature measuring point is located in the outdoor shade. The measuring point of the solar radiation intensity is arranged outdoors with no shelter. The indoor air temperature measuring point is located 1.5 m above the floor in the center of the room. The monitoring period for the solar radiation intensity measuring points is 10 h, and the acquisition time interval is 1 h. The monitoring period for the air temperature measuring points is 24 h, and the acquisition time interval is 10 min.

We are concerned that the hot wire anemometer and globe thermometer will cause inconvenience to the residents' life if they are placed indoors for a long time. Therefore, the measurements of the mean radiant temperature and air velocity are conducted by intermittent tests. The measuring points of the indoor air velocity and mean radiation temperature are placed at the height of 1.0 m above the floor in the center of the room. The main information about the test instruments is shown in Table 1.

2.3. Results and Analysis. During the test, the outdoor weather conditions were similar every day. Therefore, the test data on January 2, 2016 are selected for the following analysis.

The changes of outdoor air temperature and solar radiation intensity are shown in Figures 2 and 3, respectively.

Figure 2 shows that from 5 am to 4:00 pm, the outdoor temperature is on the rise, while from 4:00 pm to 12 pm, the outdoor temperature shows a decreasing trend. The outdoor temperature varies from 1.3°C to 6.6°C with the temperature fluctuation of 5.3°C, and the mean temperature of 3.6°C. It can be seen that the outdoor air temperature in this area is lower and the temperature fluctuation is slightly larger in winter.

Figure 3 shows that the local sunshine duration is about 10 h. The peak total radiation intensity is 500.7 W/m^2, and the average radiation intensity is 234.6 W/m^2. The direct radiation intensity accounts for 64.2% of the total radiation intensity. To conclude, the region has a long sunshine time and relatively high solar radiation intensity, which has a geographical advantage to develop solar buildings.

The changes of indoor air temperature, as shown in Table 2.

Table 2 shows the maximum, minimum, and average temperatures of the master bedrooms and the secondary bedrooms. It is obvious that the master bedrooms are higher than that of the secondary bedrooms, and the indoor temperature of the bedrooms on the second floor is lower than that on the first floor. The fluctuation range of the indoor temperature of the master and secondary bedrooms on the first floor is from 8.7°C to 12.1°C and from 8.0°C to 10.8°C, with the average temperature of 10.5°C and 9.8°C, respectively. The fluctuation range of the indoor temperature of the master and secondary bedrooms on the second floor is from 8.1°C to 12.8°C and 7.5°C to 11.6°C, with the average temperature of 10.0°C and 9.4°C, respectively. To sum up, the indoor temperature in this area is low and fluctuates greatly in winter.

Through the intermittent tests, it is found that the mean radiation temperature is approximately equal to the air temperature. The indoor air velocity varies from 0.03 m/s to 0.12 m/s, and the average value is 0.1 m/s.

In addition, we also surveyed the heating status of local rural residential buildings. It is found that the heating energy for local rural residential buildings in winter is mainly coal, and each household consumes about 3.2 *t* of coal during the heating period. Even so, most of the residents in this area are still concentrated in the same room in winter. If the residents adopt the auxiliary heating method of the compartment, the heating energy consumption will be 1.5 to 2.0 times of the existing energy consumption. The survey also shows that the percentage of the residents who are satisfied and general with the current heating method and heating effect is 14.1% and 43.7%, respectively. Besides, 42.2% of residents express dissatisfaction with the current heating method and heating effect. They think that the indoor heating energy consumption is high, but the indoor thermal comfort is still poor and the indoor air quality is low.

In summary, the indoor thermal environment of the existing local rural residential buildings is not ideal. The residents' satisfaction is low, and the heating energy consumption is high. However, this area is rich in solar energy resources and has the potential to develop solar energy buildings.

3. Design Method of Energy-Saving Wall Based on Uniform Radiation Field

3.1. Determination of Indoor and Outdoor Calculated Temperature

3.1.1. Indoor Design Calculation Temperature. The common international comfort indexes are operative temperature (To), effective temperature (ET), new effective temperature (SET*), predicted mean vote (PMV), and subjective temperature (Tsub).

Yaglon et al. [50] proposed the ET as the indoor thermal comfort evaluation index, but this index had the

Table 1: The main information about the test instruments.

Survey content	Test parameters	Test instruments	Range	Accuracy
Outdoor thermal environment	Solar radiation intensity	Solar radiometer (JTDL-4)	0~2000 (W/m^2)	±0.2°C
	Air temperature	Thermometer and hydrometer (TESTO175-H)	−20~70°C	±0.1°C
Indoor thermal environment	Air temperature	Thermometer and hydrometer (TESTO175-H)	−20~70°C	±0.1°C
	Air velocity	Hot wire anemometer (Testo425)	0~20 m/s	±0.03%
	Mean radiation temperature	Globe thermometer (JTR05)	−20°C~125°C	±0.2°C

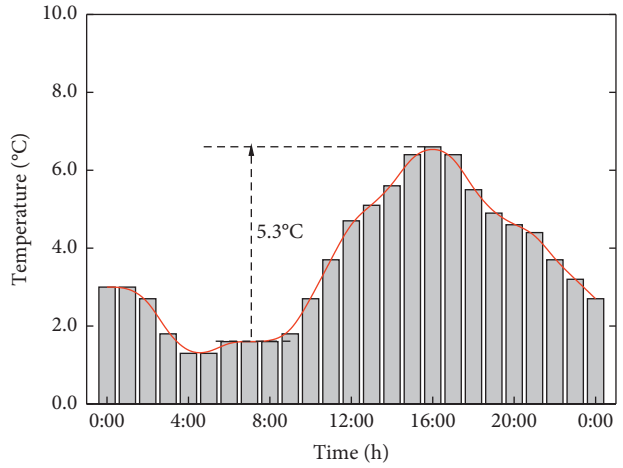

Figure 2: Outdoor air temperature curve.

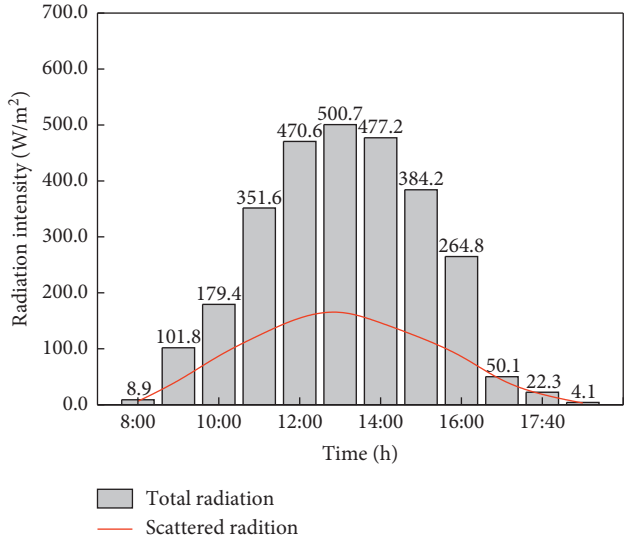

Figure 3: Solar radiation intensity curve.

Table 2: The changes of indoor temperature.

Rooms		Maximum temperature (°C)	Minimum temperature (°C)	Average temperature (°C)
Master bedrooms	First floor	12.1	8.7	10.5
	Second floor	12.8	8.1	10.0
Secondary bedrooms	First floor	10.8	8.0	9.8
	Second floor	11.6	7.5	9.4

disadvantage of estimating the impact of humidity on thermal sensation. This evaluation index is more perfect as an evaluation index when the effective temperature ET is further improved to the standard effective temperature SET*. It is inconvenient to apply to the design because it is intricate to calculate the skin temperature and wettability [51]. PMV is put forward as the evaluation index of indoor thermal comfort. Although the indicator has been considered perfect, it is difficult for most areas of China to reach the standard of PMV = –0.5~0.5, and it is also considered unnecessary in rural areas of China [52]. T_o is put forward as the evaluation index of the indoor thermal environment. However, this index can only qualitatively evaluate the indoor thermal comfort and does not guide the thermal design of buildings well [53]. Mcintyre [54] brought forward the T_{sub} as an evaluation index of the indoor thermal comfort. The T_{sub} refers to the temperature of a uniform closed environment that can produce the same thermal sensation as the actual environment. In this indoor thermal environment, the air temperature and the mean radiation temperature are equal to each other. The air velocity is 0.1 m/s, and the air relative humidity is 50%.

Based on the above analysis, it is considered that T_{sub} as the evaluation index of the indoor thermal environment is effective and feasible. Within the allowable error range, the T_{sub} can be calculated as follows [54]:

$$T_{sub} = 33.5 - 3R_{clo} - (0.08 + 0.05R_{clo}) \cdot M, \quad (1)$$

where T_{sub} is the subjective temperature; M is the metabolic rate (W/m^2); and R_{clo} is the thermal resistance of clothing, and its calculation formula is as follows [54]:

$$R_{clo} = 0.113 + 0.727 \sum R_i \quad \text{(the male)}, \quad (2)$$

$$R_{clo} = 0.05 + 0.77 \sum R_i \quad \text{(the female)}, \quad (3)$$

where R_{clo} is the total clothing thermal resistance and R_i is the thermal resistance for each piece of clothing in units of clo (1 clo = 0.155 (°C·m^2)/W).

According to the survey on the living habits and clothing of rural residents in Qinba mountains, the following conclusions can be drawn:

(1) In winter, the local rural residents are in the period of agricultural leisure. The metabolism rate of the local rural residents is calculated according to the average labor intensity. According to ASHRAE standard 55-2013 [55], the metabolism rate of the local rural residents is 85 W/m^2.

(2) According to the literature [56], combined with the dressing thickness of different genders and different ages of the local rural residents, the thermal resistance of local residents' winter clothing is 1.7 clo.

According to the above formulas (1)~(3), the T_{sub} is 14.4°C. In winter, it is suggested that the indoor thermal comfort temperature of rural buildings in Qinba mountains should not be lower than 14°C based on the comprehensive analysis of comfort, energy conservation, and economy.

3.1.2. Outdoor Calculated Temperature. The comprehensive effect of outdoor air temperature and solar radiation should be considered in the thermal calculation of buildings in areas with abundant solar energy resources. Therefore, the outdoor comprehensive temperature is more accurate than the outdoor air temperature to describe the outdoor thermal effect of different orientation envelope. The calculation formula of outdoor comprehensive temperature is as follows [57]:

$$t_{sa} = t_a + \frac{q_S + q_R}{\alpha_a} - \frac{q_e}{\alpha_a}, \quad (4)$$

where t_{sa} is the outdoor comprehensive temperature; t_a is the outdoor air temperature, °C; a_a is the total heat transfer coefficient of building wall surface with the value of 23.0 W/(m^2·°C) [57]; q_e is the effective radiation or night radiation, W/m^2; q_S is the ground reflected radiant heat absorbed by the outer surface of building envelope, W/m^2; q_R is the solar radiation heat absorbed by the outer surface of building envelope, W/m^2. The absorption rate of sunlight on the outer surface of the building envelope is 0.7 [57].

The winter solstice has the shortest sunshine time and the lowest solar altitude angle. So, it is typical to select the weather data of this day to analyze the outdoor thermal effect of buildings. On the winter solstice, the outdoor air temperature in Ankang area and the comprehensive outdoor temperature with different orientations are shown in Table 3.

3.2. Heat Transfer Coefficient of External Wall of Energy-Saving Residential Buildings

3.2.1. Heat Balance Equation of Energy-Saving Residential Buildings. In areas with abundant solar energy resources, the indoor thermal condition of buildings is not only affected by factors such as building construction mode and thermal parameters but also affected by solar radiation intensity and outdoor air temperature.

In the heating period, the indoor heat gain is composed of solar radiation heat obtained from heat collection components as well as indoor residual heat and auxiliary heat consumption. The heat loss includes the heat transfer loss of envelope and the heat consumption of air infiltration. The heat balance equation is as follows [58]:

$$\begin{aligned} \text{NLC} \cdot (\overline{T_r} - \overline{T_a}) &= \overline{Q_{cg}} + \overline{Q_{ob}} + \overline{Q_{in}} + Q_{aux}, \\ \text{NLC} &= \sum_{j=nc+1}^{nb} A_j U_j + \frac{nV_f \overline{\rho_a} c_p}{3.6}, \\ \overline{Q_{cg}} &= A_g \cdot \overline{H_{t\theta}} \cdot \eta, \\ \overline{Q_{ob}} &= \sum_{j=nc+1}^{mb} A_i U_i \overline{T_{di}}, \end{aligned} \quad (5)$$

where NLC is the static load factor of the room, W/°C; A_j is the area of the envelope j, m^2; n is the number of air changes in the room with the value of 1.0 times/h [59]; V_f is the internal volume of the room, m^3; $\overline{\rho_a}$ is the average density of

Table 3: The comprehensive outdoor temperature fluctuations (hourly) of Ankang area in the winter solstice.

Time	Outdoor comprehensive temperature (°C)				Outdoor air temperature (°C)
	South	East	West	North	
1:00	−0.13	−0.13	−0.13	−0.13	1.90
2:00	−0.93	−0.93	−0.93	−0.93	1.10
3:00	−1.22	−1.22	−1.22	−1.22	0.80
4:00	−0.92	−0.92	−0.92	−0.92	1.10
5:00	−0.33	−0.33	−0.33	−0.33	1.70
6:00	−0.03	−0.03	−0.03	−0.03	2.00
7:00	−0.32	−0.32	−0.32	−0.32	1.70
8:00	−0.91	−0.91	−0.91	−0.91	1.10
9:00	−0.10	−0.06	−0.33	−0.33	0.70
10:00	1.42	1.33	0.98	0.98	0.80
11:00	4.06	3.56	3.11	3.11	1.70
12:00	8.97	6.33	5.76	5.76	3.20
13:00	14.18	7.81	8.52	7.81	5.10
14:00	13.91	9.47	11.27	9.47	7.20
15:00	18.67	9.94	16.28	9.94	8.80
16:00	16.27	9.68	16.93	9.68	9.70
17:00	8.59	7.85	9.00	7.85	9.40
18:00	6.20	6.20	6.20	6.20	8.40
19:00	5.14	5.14	5.14	5.14	7.30
20:00	4.57	4.57	4.57	4.57	6.70
21:00	4.58	4.58	4.58	4.58	6.70
22:00	4.48	4.48	4.48	4.48	6.60
23:00	3.98	3.98	3.98	3.98	6.10
0:00	3.49	3.49	3.49	3.49	5.60

outdoor air with the value of 1.27 kg/m^3 [59]; c_p is the constant pressure specific heat capacity of air with the value of 1.008 kJ/(kg·°C) [59]; $\overline{T_r}$ is the calculated temperature of indoor air, °C; $\overline{T_a}$ is the calculated temperature of outdoor air, °C; $\overline{Q_{cg}}$ is the monthly average daily radiation of the total daily solar radiation transmitted to the room by the rest of the envelope except the heat collecting component of the room, W; $\overline{Q_{in}}$ is the average value of heat generated by indoor people, lighting and non-dedicated heating equipment in the room, W; Q_{aux} is the auxiliary heat consumption, W; A_g is the window area of the heat collecting component, m^2; $\overline{H_{t\theta}}$ is the total average daily radiation amount projected on the window surface, W/m^2; η is the efficiency of the heat collecting component with the value of 0.13 [59]; $\overline{T_{di}}$ is the equivalent temperature of the outdoor solar radiation and the long-wave effective radiation of the envelope i, °C.

3.2.2. Analysis of External Wall Heat Transfer Coefficient. According to formula (5), the calculation formula of net average heat transfer coefficient of external wall is obtained, as shown in the following formula:

$$\sum_{j=nc+1}^{mb} A_j U_j \left(\overline{T_r} - \overline{T_a}\right) + \sum_{j=mb+1}^{nb} A_j U_j \left(\overline{T_r} - \overline{T_a}\right) + \frac{nV_f \overline{\rho_a} c_p \left(\overline{T_r} - \overline{T_a}\right)}{3.6} = A_g \cdot \overline{H_{t\theta}} \cdot \eta + \sum_{j=nc+1}^{mb} A_j U_j \overline{T_{di}} + \overline{Q_{in}} + Q_{\text{aux}}, \tag{6}$$

where $\overline{T_{saj}} = \overline{T_a} + \overline{T_{di}}$, $\overline{T_{saj}}$ is the outdoor comprehensive temperature of the envelope j, °C; mb is the number of external walls and roof; and nb-mb is the total number of external doors and windows of nonheat collecting components.

(1) Characteristics of Representative Rural Residential Buildings in Ankang Area. According to the literature [60] and our field survey, the plans and basic parameters of the representative rural residential buildings in Ankang area are determined, as shown in Figure 4 and Table 4, respectively.

(2) Correlation Analysis of External Wall Heat Transfer Coefficient Based on Uniform Radiation. Many scholars have studied the influence of indoor nonuniform radiation on human thermal comfort. The results show that asymmetric radiation temperature has a significant adverse effect on human thermal comfort. For the rural buildings with strong solar radiation in Qinba mountains, the discomfort of the human body caused by the indoor nonuniform radiation field will be more serious if the same thermal parameters are adopted for the enclosure structures with different orientations. Therefore, it is an effective way to reasonably determine the thermal resistance of envelopes with different orientations to solve the problems of indoor comfort and energy saving of rural buildings.

Taking the indoor calculated temperature and the comprehensive temperature of the air in different orientations as the boundary conditions, the correlation of the heat transfer resistance for each orientation of the external wall is analyzed based on the principle of uniform radiation, as shown in the following equations:

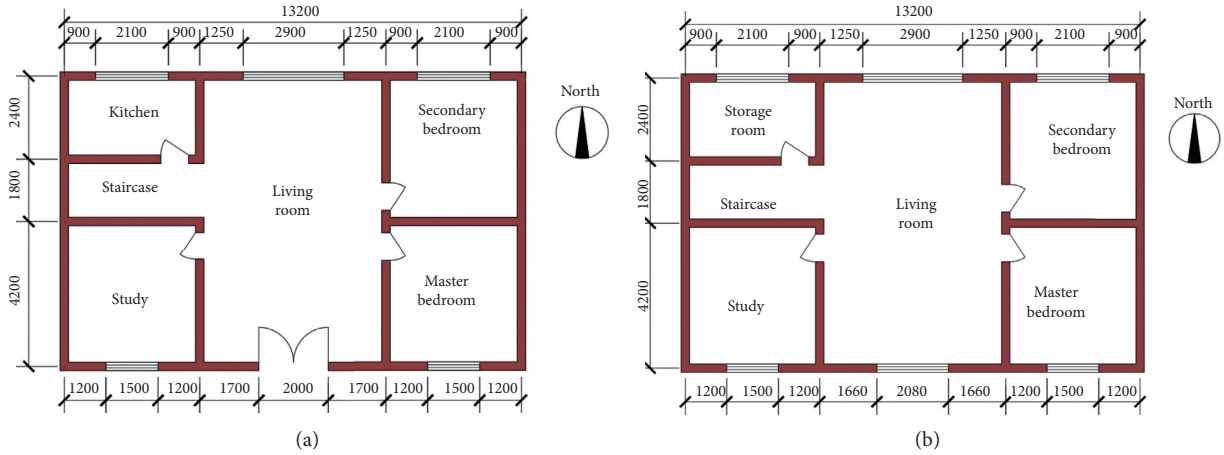

Figure 4: Plans of the representative rural buildings in Ankang area. (a, b) First floor plan of the representative rural buildings.

Table 4: Basic structural parameters of the representative rural buildings in Ankang area.

Building height (m)	Heat transfer coefficient (W/(m^2·k))		Surface area of the building envelope (m^2)								Building volume (m^3)
	External wall	Partition wall	Roof	South		East-west Wall	North		Door	Roof/ Floor	
				Window	Wall		Window	Wall			
3.3	2.04	3.11	3.70	12.87 —	12.85 —	27.72	— 13.07	— 30.49	3.78	99.58	365.90

Note. The external window is a plastic single-frame double glass window (4 + 12A + 4), and the heat transfer coefficient is 2.2 W/(m2·°C) [61]. The external door is an aluminum alloy energy-saving door with a heat transfer coefficient of 2.5 W/(m^2·°C) [61].

$$\theta_i = \theta_{i\cdot S} = \theta_{i\cdot E} = \theta_{i\cdot W} = \theta_{i\cdot N}, \tag{7}$$

where $\theta_{i.S}$, $\theta_{i.E}$, $\theta_{i.W}$, and $\theta_{i.N}$ are the inner surface temperature of the south, east, west, and north walls, respectively, °C:

$$\theta_i = \overline{T_r} - \frac{R_i}{R_{oj}}\left(\overline{T_r} - \overline{T_{saj}}\right), \tag{8}$$

where $\overline{T_r}$ is the indoor design calculation temperature, °C; R_{oj} is the heat transfer resistance to external walls and roofs with different orientations, (m^2·K)/W; and $\overline{T_{saj}}$ is the comprehensive outdoor temperature corresponding to the envelope, °C.

From equations (7)~(8) and Table 3, the correlation of the heat transfer coefficients of external walls with different orientations can be obtained:

$$U_S = 1.13U_E = 1.06U_W = 1.14U_N, \tag{9}$$

where U_j is the heat transfer coefficient of external walls with different orientations, W/(m^2·K).

It can be seen from equation (9) that the heat transfer coefficient of the external walls with different orientations has a quantitative proportional relationship. In order to simplify the calculation process, the heat transfer coefficient U_S of the south wall is determined as the basic heat transfer coefficient.

(3) Analysis of Relationship between Auxiliary Heat Consumption and Heat Transfer Coefficient of External Wall. The relationship between the basic heat transfer coefficient and the auxiliary heat consumption can be obtained by taking the indoor and outdoor calculated temperature obtained from the above analysis and the basic parameters of Table 4 into equations (6) and (9), as shown in equation (10) and Figure 5:

$$U_S = \frac{Q_{\text{aux}} - 1279.51}{1840.12}. \tag{10}$$

Figure 5 shows that the basic heat transfer coefficient has a linear relationship with indoor auxiliary heat consumption. Therefore, for the rural residential buildings which have determined the basic parameters, window wall ratio, and window materials, it is an effective method to reduce the building energy consumption by reasonably controlling the basic heat transfer coefficient of the external wall of the building.

The literature [59] shows that the heat consumption of rural residential buildings in Qinba Mountains during the winter solstice is 61.54 W/m^2 under the state of natural operation state. It can be seen from Figure 2 that, under the premise of building energy saving of 50%, the basic heat transfer coefficient of the external wall of rural residential buildings in Qinba mountains is 0.9 W/(m^2·K). The heat transfer coefficients of external walls with different orientations are as shown in Table 5.

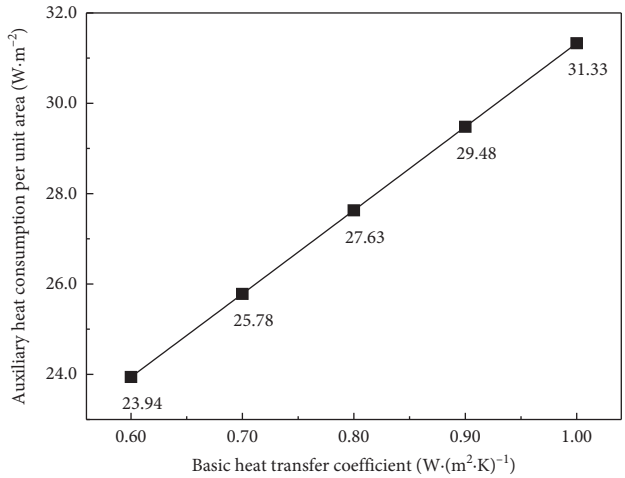

Figure 5: The relationship between the basic heat transfer coefficient and auxiliary heat consumption.

Table 5: The heat transfer coefficient of the enclosure structure based on the uniform radiation field.

Thermal parameters	South wall	East wall	West wall	North wall
Heat transfer coefficient (W·(m^2·K)$^{-1}$)	0.90	0.80	0.85	0.80
Heat transfer resistance ((m^2·K)·W^{-1})	0.96	1.10	1.03	1.10

4. Structure Suitability Analysis of Energy-Saving Wall

4.1. Selection of Numerical Analysis. Many engineering problems can be summarized as the mathematical problems of solving the control equations under given boundary conditions. However, only a few problems in which the properties of the equations are relatively simple and the geometric boundary conditions are quite regular can be solved analytically. Thus, many researchers have developed effective numerical methods, such as finite element method (FEM) [62, 63], meshless method [64–66], and boundary element method (BEM) [67, 68], when it is impossible to solve engineering problems by the analytical method.

The BEM is to divide the unit only on the boundary of the definition domain and use the function that meets the control equation to approximate the boundary conditions. The boundary element method reduces the dimensions of the problem by one degree, which leads to significant advantages in terms of ease of discretization of the domain and of reducing the overall time to perform the analysis of objects with complex geometries. Although BEM can save the preprocessing time, it requires a basic solution when establishing boundary integral equations, and the singular integral of boundary integral equation is difficult to solve complex structural problems [62]. As an alternative to mesh-based methods, meshless methods have attracted much attention in recent years due to (1) the lack of dependence on mesh and avoiding meshing; (2) remeshing and mesh distortion (in large deformation problems); and (3) easy preparation of the initial data. Meshless methods are used to establish a system of algebraic equations for the whole problem domain without the use of a predefined mesh. Meshless methods use a set of nodes scattered within the problem domain as well as sets of nodes scattered on the boundaries of the domain to represent the problem domain and its boundaries. These sets of scattered nodes do not form a mesh, which means that no information on the relationship between the nodes is required, at least for field variable interpolation. Because there is no need to create a mesh and the nodes can be created by a computer in a fully automated manner, the time an engineer would spend on conventional mesh generation can be saved. This can translate to substantial cost and time savings in modeling and simulation projects. But meshless methods developed so far are not really ideal and fail in some categories. For example, some meshless methods require background cells for the integration of system matrices derived from the weak form over the problem domain, and some methods that do not require a mesh at all are less stable and less accurate [68].

The FEM as a general discretization procedure of continuum problems posed by mathematically defined statements has been one of the major numerical solution techniques. The finite element method requires division of the problem domain where the partial differential governing equations are defined into meshes, and each mesh is called a finite element. The FEM not only has high calculation accuracy but also can be applied to various complex geometric models, complex material characteristics, and complex boundary conditions. Another major advantage of the finite element method is that a general purpose computer program can be developed easily to analyze various kinds of problems.

In the field of architecture, ANSYS CFX is one of the most comprehensive and universal finite element analysis software. The software has general physical models including flow, heat transfer, and radiation. The software adopts the element-based finite volume method and absorbs the numerical accuracy of the finite element method. Therefore, ANSYS CFX was adopted for the follow-up study in this paper.

4.2. Model Establishment

4.2.1. Mathematical Model. The model is controlled by the k~ε equation of turbulent natural convection [69] and the IMMERSOL (IMMER sed SOLids) equation of Stefan–Boltzmann law [70]:

(1) Standard k~ε model:

$$k \text{ equation: } \frac{\partial}{\partial t}(\rho k) + \frac{\partial}{\partial x_i}(\rho k \mu_i) = \frac{\partial}{\partial x_j}\left[\left(\mu + \frac{\mu_i}{\sigma k}\right)\frac{\partial k}{\partial x_j}\right] + Gk + Gb - \rho\varepsilon - Ym + Sk, \tag{11}$$

$$\varepsilon \text{ equation: } \frac{\partial}{\partial t}(\rho \varepsilon) + \frac{\partial}{\partial x_j}(\rho \varepsilon \mu i) = \frac{\partial}{\partial x_j}\left[\left(\mu + \frac{\mu_i}{\sigma \varepsilon}\right)\frac{\partial \varepsilon}{\partial x_j}\right] + G1\varepsilon\frac{\varepsilon}{k}(Gk + C3\varepsilon Gb) - C2\varepsilon\rho\frac{\varepsilon^2}{k} + S, \tag{12}$$

where Gk is the turbulent kinetic energy generated by the laminar velocity gradient, J; Gb is the turbulent kinetic energy generated by buoyancy, J; Ym is the fluctuation caused by the transitional diffusion; ∂_j is the turbulent Prandtl number of the j equation; $C1$, $C2$, and $C3$ all are constants; S is a custom physical quantity; k is turbulent pulsating kinetic energy, J; ε is the dissipation rate of turbulent pulsating kinetic energy, %.

(2) IMMERSOL (IMMER sed SOLids) model of Stefan–Boltzmann law.

When T_3 is the solid temperature, the equation is as follows:

$$c \times \frac{dT_3}{dt} = \operatorname{div}(\lambda \times \operatorname{grad} T_3) + q, \tag{13}$$

where c is the specific heat capacity of the solid, J/kg·W; λ is the thermal conductivity of the solid, W/m·K; q is the heat flux per unit volume of the solid, W/kg; and t is the time, s.

When T_3 is the radiation temperature between solids, the equation is as follows:

$$\operatorname{div}\left[\frac{\operatorname{grad} E_3}{0.75} \times \left(\alpha + S + \frac{1}{L}\right)\right] = (\alpha + S) \times (E_{12} - E_3), \tag{14}$$

where E_3 is the net value of the radiant energy gained or lost per unit volume, W/m^2; E_{12} is the average radiant force of the first and second fluid surface, W/m^2; a is the absorptivity of the medium; S is the scattering coefficient of the medium; and L is the distance between two solid radiation surfaces, s.

4.2.2. Physical Model. The physical model of representative rural residential buildings in Ankang area is shown in Figure 6.

In order to facilitate the numerical simulation, the physical model is simplified as follows: (1) the indoor air body of all the rooms is considered as a whole; (2) the external envelope and internal partition lines are assumed to be isotropic one-dimensional thermal conductors whose thermal parameters are calculated by the weighted average of the thermal parameters of each material layer; (3) the influence of external door, window type, and cold air infiltration on the indoor air temperature is ignored; (4) the indoor door is set default to be open, the external door and window to be closed, and the bright window part of the external door to be vent; (5) the influence of indoor human activities on the indoor air temperature is ignored; (6) the sloping roof is simplified to a flat roof with an air layer.

4.3. Mesh Generation. In order to simplify the calculation process of the model, only key parts such as external walls, roofs, doors, and windows are encrypted in the study. The size of the calculating model is given in Figure 4 and Table 4. The total number of the grid formed is 306036, and the minimum grid size is 0.02 m. The physical model of the encrypted building is shown in Figure 7.

4.4. Parameter Setting. Through field survey, it is found that the external walls of rural residential buildings in Ankang area are mostly 240-mm-thick solid clay brick walls without thermal insulation layer. A few buildings also adopt sandwich insulation walls with solid clay brick, limes and brick, and KP1 porous brick. According to the thermal design method of the wall proposed above, combined with the materials and their combination modes of the local rural building walls, three typical energy-saving structural walls are selected to conduct analysis in this paper, which are category I, category II, and category III, respectively. Category I is an energy-saving structural wall with KPI porous brick as the main material and a basic heat transfer coefficient of 0.9 W/(m^2·K). Category II is an energy-saving structural wall with KPI porous brick as the main material and a basic heat transfer coefficient of 0.9 W/(m^2·K). Category III is an energy-saving structural wall with KPI porous brick as the main material and a basic heat transfer coefficient of 0.9 W/(m^2·K). The construction methods and thermal parameters of different categories of energy-saving walls are shown in Table 6.

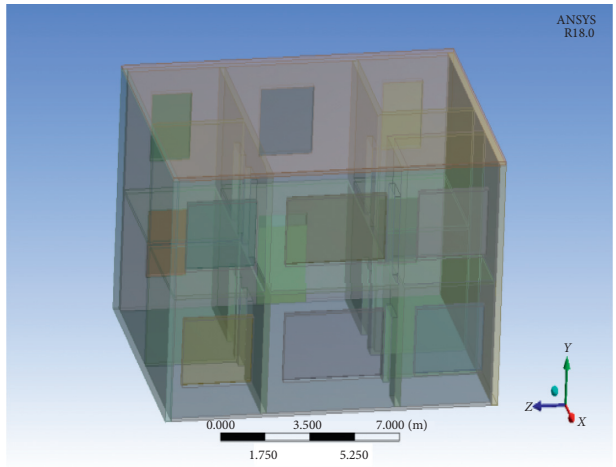

Figure 6: Three-dimensional physical model of representative rural residential building in Ankang area.

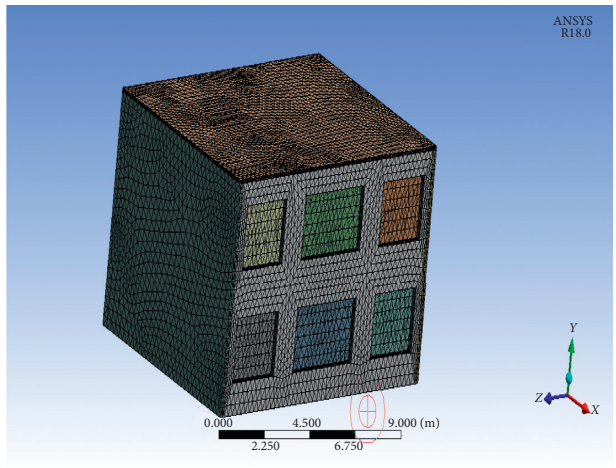

Figure 7: The physical model of the encrypted building.

4.5. Setting of Boundary Conditions. Under the premise that indoor temperature is a certain value, the unstable heat transfer of building envelope is determined by the change of the outdoor disturbance and the response of the envelope to the external disturbance. The outdoor disturbances, such as outdoor air temperature and solar radiation intensity acting on the building envelope, take 24 hours or 365 days as a cycle. Although the meteorological conditions generally show periodic changes, the changes are random and irregular. Because the complex disturbance curve can be expressed as a group of simple periodic functions by using the Fourier series expansion (formula (15)), the outdoor comprehensive temperature described by the Fourier function is used in this research:

$$t_z(\tau) = A_o + \sum_{n=1}^{\infty} A_n \sin(n\omega\tau + \varphi_n), \tag{15}$$

where A_o is the zero-order outdoor disturbance, which is considered to be the average value of the outdoor comprehensive temperature in the calculation period; A_n is the amplitude of the outdoor disturbance of the n-th sine wave; $n\omega$ is the frequency of the external disturbance of the n-th sine wave, $n\omega = 2\pi n/T$ (rad); φ_n is the initial phase of the external disturbance of the n-th sine wave; and τ is the period of the function, h.

In the calculation of the building heat transfer process, the sampling interval of outdoor disturbance is 1 h, j is the sequence number of sampling value, and n is the order of harmonic with the value of 4. The expression of harmonic function is as follows:

$$t_z(j\Delta\tau) = A_0 + \sum_{n=1}^{\infty} A_n \sin(n\omega j\Delta\tau + \varphi_n). \tag{16}$$

According to Table 3 and formula (16), the fourth-order Fourier series expression of outdoor comprehensive temperature in different orientations on the winter solstice in Ankang area is obtained.

The comprehensive outdoor temperature function in south orientation $t_{sa\cdot S}$ is as follows:

Table 6: The construction modes and thermal parameters of energy-saving wall.

Name	Project	Material	Thickness (mm)	Thermal conductivity (W/(m·K))	Dry density (kg/m^3)	Heat transfer coefficient (W/(m^2·k))
Category I	South wall	Cement mortar (internal and external)	20 + 20	0.93	1800	0.9
		Solid clay brick	240	0.81	1900	
		EPS	28	0.041	18	
	East wall	Cement mortar (internal and external)	20 + 20	0.93	1800	0.8
		Solid clay brick	240	0.81	1900	
		EPS	34	0.041	18	
	West wall	Cement mortar (internal and external)	20 + 20	0.93	1800	0.85
		Solid clay brick	240	0.81	1900	
		EPS	31	0.041	18	
	North wall	Cement mortar (internal and external)	20 + 20	0.93	1800	0.8
		Solid clay brick	240	0.81	1900	
		EPS	34	0.041	18	
Category II	South wall	Cement mortar (internal and external)	20 + 20	0.93	1800	0.9
		Lime sand brick	240	1.100	1900	
		EPS	31	0.041	25	
	East wall	Cement mortar (internal and external)	20 + 20	0.93	1800	0.8
		Lime sand brick	240	1.100	1900	
		EPS	38	0.041	25	
	West wall	Cement mortar (internal and external)	20 + 20	0.93	1800	0.85
		Lime sand brick	240	1.100	1900	
		EPS	34	0.030	25	
	North wall	Cement mortar (internal and external)	20 + 20	0.93	1800	0.8
		Lime sand brick	240	1.100	1900	
		EPS	38	0.041	25	
Category III	South wall	Cement mortar (internal and external)	20 + 20	0.93	1800	0.9
		KP1 porous brick	240	0.58	1600	
		EPS	23	0.041	18	
	East wall	Cement mortar (internal and external)	20 + 20	0.93	1800	0.8
		KP1 porous brick	240	0.58	1600	
		EPS	29	0.041	18	
	West wall	Cement mortar (internal and external)	20 + 20	0.93	1800	0.85
		KP1 porous brick	240	0.58	1600	
		EPS	26	0.041	18	
	North wall	Cement mortar (internal and external)	20 + 20	0.93	1800	0.8
		KP1 porous brick	240	0.58	1600	
		EPS	29	0.041	18	

Note. According to the literature [71], the heat transfer resistance for the inner surface of the wall is 0.11 (m^2·k)/W. The heat transfer resistance of the inner surface of the wall is 0.04 (m^2·k)/W, and the thermal conductivity correction coefficient of the insulation layer is 1.1.

$$t_{sa.S(\tau)} = 4.7 + 7.0167 \sin\left(\frac{\pi}{12}\tau + 3.7357\right) + 3.0627 \sin\left(\frac{\pi}{6}\tau + 0.3954\right) + 2.5353 \sin\left(\frac{\pi}{4}\tau + 2.8359\right) + 0.4178 \sin\left(\frac{\pi}{3}\tau + 4.3601\right). \quad (17)$$

The comprehensive outdoor temperature function in south orientation $t_{sa\cdot E}$ is

$$t_{sa.E(\tau)} = 3.5 + 4.8927 \sin\left(\frac{\pi}{12}\tau + 3.5682\right) + 1.1911 \sin\left(\frac{\pi}{6}\tau + 0.5243\right) + 1.2650 \sin\left(\frac{\pi}{4}\tau + 2.9131\right) + 0.4420 \sin\left(\frac{\pi}{3}\tau + 2.5141\right). \quad (18)$$

The comprehensive outdoor temperature function in south orientation $t_{sa.W}$ is

$$t_{sa.W(\tau)} = 4.1 + 6.2322 \sin\left(\frac{\pi}{12}\tau + 3.0653\right) + 2.3717 \sin\left(\frac{\pi}{6}\tau + 0.1049\right) + 2.2533 \sin\left(\frac{\pi}{4}\tau + 2.5014\right) + 0.9370 \sin\left(\frac{\pi}{3}\tau + 3.8372\right). \quad (19)$$

The comprehensive outdoor temperature function in south orientation $t_{sa\cdot N}$ is

$$t_{sa.N(\tau)} = 3.4 + 4.8795 \sin\left(\frac{\pi}{12}\tau + 3.5414\right) + 1.2075 \sin\left(\frac{\pi}{6}\tau + 0.4287\right) + 1.3490 \sin\left(\frac{\pi}{4}\tau + 2.8836\right) + 0.3785 \sin\left(\frac{\pi}{3}\tau + 2.4847\right). \quad (20)$$

4.6. Model Verification. The accuracy of numerical simulation is affected by the setting of boundary conditions, the density of mesh division, and the convergence of iteration. Therefore, it is necessary to verify the accuracy of the model. The comparison between the measured data and the simulated data is shown in Figure 8.

Figure 8 shows that the variation trend of the simulation results is generally consistent with the measured data, and the relative error between them is within 8%. The main reasons for the error are the simplification of the physical model before the numerical simulation and the accuracy errors of the testing instruments. Therefore, it is effective and feasible for the physical model to be applied in the following numerical simulation analysis.

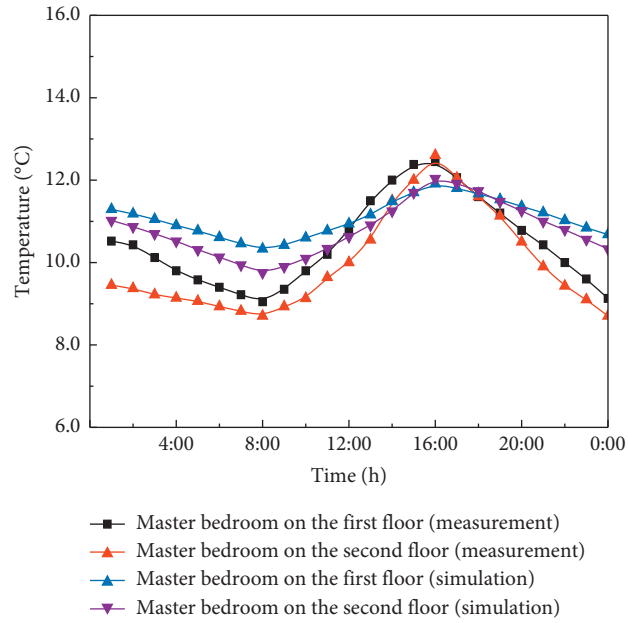

Figure 8: The comparison between the measured results and the simulated results.

4.7. Results and Analysis. The energy-saving walls with the same heat transfer coefficient but different construction methods or construction materials have different storage and release capacity for heat energy. Therefore, this paper studies the structural suitability of energy-saving wall through the analysis of indoor temperature field.

Taking the above three energy-saving walls as examples, the indoor temperature of rooms on different floors is simulated. The indoor temperature of the numerical simulation is compared with the indoor temperature of the test, and the results are shown in Figure 9.

Figure 9 shows that the energy-saving walls with the same heat transfer coefficient but different construction methods or construction materials have significantly different effects on indoor temperature. Compared with the original buildings, the indoor temperature of the buildings with the above energy-saving external wall is significantly improved, and the fluctuation of the indoor temperature is slightly reduced.

When the construction method of building wall adopts category I, the average indoor temperature of the master bedroom and the secondary bedroom on the first floor increased by 13.3% and 15.3%, respectively, reaching 11.9°C and 11.3°C. The average indoor temperature of the master bedroom and the secondary bedroom on the second floor rose by 11.0% and 13.3%, respectively, reaching 11.1°C and 10.65°C. When the construction method of building wall adopts category II, the average indoor temperature of the master bedroom and the secondary bedroom on the first floor increased by 12.4% and 13.3%, respectively, reaching 11.8°C and 11.1°C. The average indoor temperature of the master bedroom and the secondary bedroom on the second floor rose by 8.7% and 11.7%, respectively, reaching 11.1°C and 10.65°C.

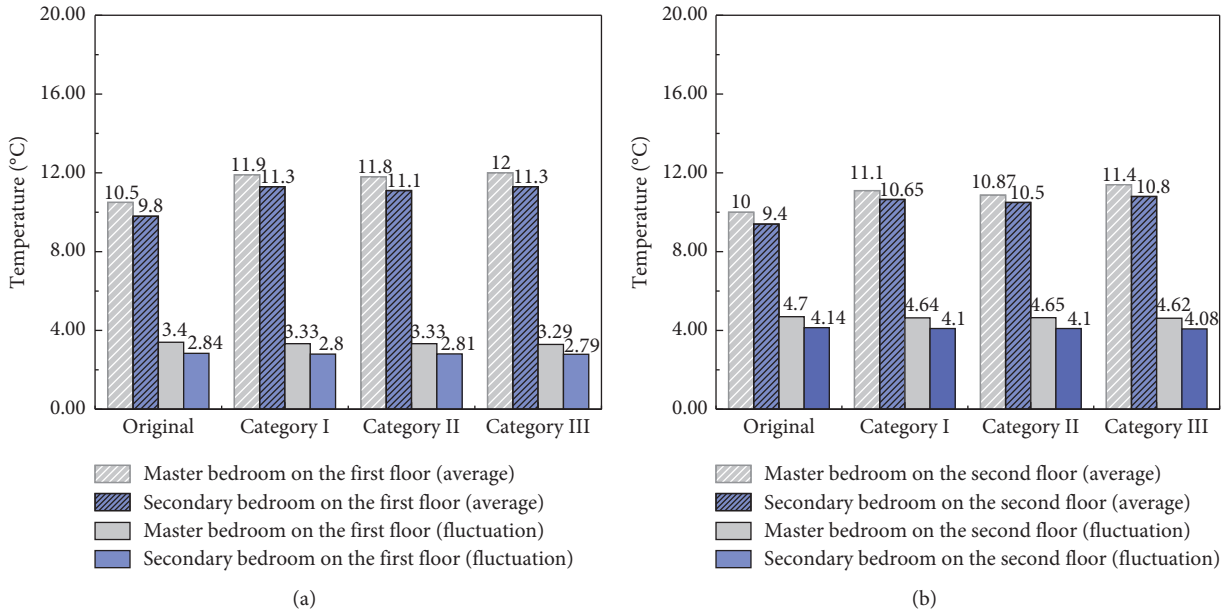

Figure 9: The influence of different materials and their combination modes of energy-saving walls on indoor temperature. Indoor temperature on (a) the first floor and (b) the second floor.

Compared with category I and category II, when the construction method of building wall adopts category III, the indoor temperature increase of each room reaches the maximum. The average indoor temperature of the master bedroom and secondary bedroom on the first floor increases by 14.3% and 15.3%, respectively, reaching 12.0°C and 11.3°C. The average indoor temperature of the master bedroom and secondary bedroom on the second floor increases by 14.0% and 14.9%, respectively, reaching 11.4°C and 10.8°C. These temperature indexes are close to the lower limit of indoor comfort temperature of the rural residential buildings in winter [17]. It can be seen that, under the climatic conditions of the Qinba mountains, the indoor thermal comfort can be significantly improved and the building energy consumption can be effectively reduced when the energy-saving structural wall with KPI porous brick as the main material and the heat transfer coefficient of the south wall of 0.9 W/(m^2·K) is selected.

5. Conclusion

(1) In winter, the indoor thermal environment of rural residential buildings in Qinba mountains is not ideal and the heating energy consumption is large. However, this area is relatively rich in solar energy resources and has the geographical advantage to develop solar energy buildings.

(2) According to the climatic conditions of Qinba mountains and the living habits of local rural residents, it is suggested that the indoor thermal comfort temperature of rural residential buildings in winter should not be lower than 14°C.

(3) When the internal surface temperature of the external walls in different orientations are equally based on the design principle of uniform radiation field, the heat transfer coefficient of the east wall, the west wall, and the north wall of the local rural residential buildings are 1.13 times, 1.06 times, and 1.14 times of the south wall heat transfer coefficient, respectively.

(4) The indoor temperature of the buildings with the energy-saving wall is significantly improved. When the main material of the energy-saving wall is KP1 porous brick and the heat transfer coefficient of the south wall is 0.9 W/(m^2·K), the average indoor temperature of the master bedroom and secondary bedroom on the first floor increases by 14.3% and 15.3%, respectively, reaching 12.0°C and 11.3°C. Besides, the average indoor temperature of the master bedroom and secondary bedroom on the second floor increases by 14.0% and 14.9% respectively, reaching 11.4°C and 10.8°C.

Data Availability

All the data and models used to support the findings of this study are included within the paper.

Conflicts of Interest

The authors declare no conflicts of interest regarding the publication of this paper.

Acknowledgments

This research was supported by the National Natural Science Foundation of China (Grant no. 51678483).

References

[1] S. P. Corgnati, M. Filippi, and S. Viazzo, "Perception of the thermal environment in high school and university classrooms: subjective preferences and thermal comfort," *Building and Environment*, vol. 42, no. 2, pp. 951–959, 2007.

[2] D. G. Valeria, D. P. Osvaldo, and D. C. Michele, "Indoor environmental quality and pupil perception in Italian primary schools," *Building and Environment*, vol. 56, no. 335, pp. 335–345, 2012.

[3] N. E. Klepeis, W. C. Nelson, W. R. Ott et al., "The nationalhuman activity pattern survey (NHAPS): a resource for assessing exposure to environment pollutants," *Journal of Exposure Analysis and Environment Epidemiology*, vol. 11, no. 335, pp. 231–252, 2001.

[4] C. P. Le, N. Bonvallot, P. Glorennecet et al., "Indoor environment and children's health: recent developments in chemical, biological, physical and social aspects," *International Journal of Hygiene and Environmental Health*, vol. 215, no. 1, pp. 1–18, 2011.

[5] F. Wu, D. Jacobs, C. Mitchell, D. Miller, and M. H. Karol, "Improving indoor environmental quality for public health: impediments and policy recommendations," *Environmental Health Perspectives*, vol. 115, no. 6, pp. 953–957, 2007.

[6] O. Hänninen, R. Sorjamaa, P. Lipponen, J. Cyrys, T. Lanki, and J. Pekkanen, "Aerosol-based modelling of infiltration of ambient PM2.5 and evaluation against population-based measurements in homes in Helsinki, Finland," *Journal of Aerosol Science*, vol. 66, no. 1, pp. 111–122, 2013.

[7] R. Pacheco, J. Ordóñez, and G. Martínez, "Energy efficient design of building: a review," *Renewable and Sustainable Energy Reviews*, vol. 16, no. 6, pp. 3559–3573, 2012.

[8] W. He, Q. Y. Jiang, J. Ji, and W. Wei, "A study on thermal performance, thermal comfort in sleeping environment and solar energy contribution of solar Chinese Kang," *Energy and Buildings*, vol. 58, no. 3, pp. 66–75, 2013.

[9] D. Song and Y.-J. Choi, "Effect of building regulation on energy consumption in residential buildings in Korea," *Renewable and Sustainable Energy Reviews*, vol. 16, no. 1, pp. 1074–1081, 2012.

[10] G. Liu, S. Zheng, P. Xu, and T. Zhuang, "An ANP-SWOT approach for ESCOs industry strategies in Chinese building sectors," *Renewable and Sustainable Energy Reviews*, vol. 93, no. 1, pp. 90–99, 2018.

[11] T. Huo, H. Ren, X. Zhang et al., "China's energy consumption in the building sector: a Statistical Yearbook-Energy Balance Sheet based splitting method," *Journal of Cleaner Production*, vol. 185, no. 6, pp. 665–679, 2018.

[12] Y. Zhang, C.-Q. He, B.-J. Tang, and Y.-M. Wei, "China's energy consumption in the building sector: a life cycle approach," *Energy and Buildings*, vol. 94, no. 5, pp. 240–251, 2015.

[13] M. Evans, S. Yu, B. Song, Q. Deng, J. Liu, and A. Delgado, "Building energy efficiency in rural China," *Energy Policy*, vol. 64, no. 1, pp. 243–251, 2014.

[14] M. Shan, P. Wang, J. Li, G. Yue, and X. Yang, "Energy and environment in Chinese rural buildings: situations, challenges, and intervention strategies," *Building and Environment*, vol. 91, no. 9, pp. 271–282, 2015.

[15] B.-j. He, L. Yang, M. Ye, B. Mou, and Y. Zhou, "Overview of rural building energy efficiency in China," *Energy Policy*, vol. 69, no. 4, pp. 385–396, 2014.

[16] World Bank, *China 2030: Building a Modern, Harmonious, and Creative High Income Society*, World Bank Publications, Washington, DC, USA, 2013.

[17] M. Ma, W. Cai, and Y. Wu, "China act on the energy efficiency of civil buildings (2008): a decade review," *Science of The Total Environment*, vol. 651, no. 2, pp. 42–60, 2018.

[18] L. Jiang, X. P. Chen, and B. Xue, "Features, driving forces and transition of the household energy consumption in China: a review," *Sustainability*, vol. 11, no. 4, pp. 1–20, 2019.

[19] Y. Y. Zhu, X. N. Fan, G. C. Sang, Q. Zhao, and X. L. Cui, "Study on indoor thermal environment of rural dwellings in Northwest China in winter," *Journal of Physics: Conference Series*, vol. 1176, no. 4, pp. 1–9, 2019.

[20] S. Mirrahimi, M. F. Mohamed, L. C. Haw, N. L. N. Ibrahim, W. F. M. Yusoff, and A. Aflaki, "The effect of building envelope on the thermal comfort and energy saving for high-rise buildings in hot-humid climate," *Renewable and Sustainable Energy Reviews*, vol. 53, no. 1, pp. 1508–1519, 2016.

[21] N. Prescott, "Energy saving through building insulation and airtightness," *Proceedings of the Institution of Civil Engineers - Energy*, vol. 161, no. 2, pp. 51–55, 2008.

[22] L. Zhang and Q. F. Shi, "The comparison of energy saving characteristic of traditional residential envelope structure in southeastern shanxi," *Applied Mechanics and Materials*, vol. 409-410, no. 1, pp. 624–629, 2013.

[23] S. Lu, X. Tang, L. Ji, and D. Tu, "Research on energy-saving optimization for the performance parameters of rural-building shape and envelope by TRNSYS-GenOpt in hot summer and cold winter zone of China," *Sustainability*, vol. 9, no. 2, p. 294, 2017.

[24] Y. Z. Tian and Y. Yu, "Analysis of anshan existing residential building exterior wall energy saving reconstruction," *Advanced Materials Research*, vol. 1004-1005, no. 1, pp. 1565–1569, 2014.

[25] X. N. Fan, Y. Y. Zhu, and G. C. Sang, "Optimization design of enclosure structure of solar energy building in Northwest China based on indoor zoning," *Advances in Engineering Research*, vol. 143, no. 1, pp. 30–40, 2017.

[26] J. Zhang and S. F. Dong, "Comprehensive measures should be taken for exterior window thermal insulating energy-saving," *Applied Mechanics and Materials*, vol. 361-363, no. 1, pp. 327–330, 2013.

[27] R. Broun, H. Babaizadeh, A. Zakersalehi, and G. Menzies, "Integrated life cycle energy and greenhouse gas analysis of exterior wall systems for residential buildings," *Sustainability*, vol. 6, no. 12, pp. 8592–8603, 2014.

[28] X. Wang, N. Wang, X. Liu, and R. Shi, "Energy-saving analysis for the modern wing of the art institute of chicago and green city strategies," *Renewable and Sustainable Energy Reviews*, vol. 73, no. 6, pp. 714–729, 2017.

[29] T. Nakaya, M. Yamasaki, and Y. Sasaki, "Influence of wall composition on thermal environment of wooden houses," *Journal of Wood Science*, vol. 60, no. 2, pp. 117–126, 2014.

[30] B. Yu, J. Hou, W. He et al., "Study on a high-performance photocatalytic-Trombe wall system for space heating and air purification," *Applied Energy*, vol. 226, no. 9, pp. 365–380, 2018.

[31] X. L. Cui, Y. K. Zhang, G. C. Sang et al., "Coupling effect of space-arrangement and wall thermal resistance on indoor thermal environment of passive solar single-family building in tibet," *Applied Sciences*, vol. 9, no. 17, pp. 1–19, 2019.

[32] JGJ26-95, *Energy Conservation Design Standard for Heating Residential Buildings*, China Architecture Building Press, Beijing, China, 1996.

[33] J. I. Jiménez and Y. Castro, "Solar radiation on sloping surfaces with different orientations in granada, Spain," *Solar Energy*, vol. 28, no. 3, pp. 257–262, 1982.

[34] M. Alabiso, F. Parrini, and R. Sidri, "Hourly solar radiation on Sloping planes with different orientations from measured daily radiation on the horizontal surfaces," *Environmental Software*, vol. 4, no. 1, pp. 35–40, 1989.

[35] Y. Y. Zhu, Y. F. Liu, and J. P. Liu, "Thermal design of energy saving buildings in rural areas of northwest under the indoor uniform radiation filed," *Acta Energiae Solaris Sinica*, vol. 32, no. 7, pp. 1034–1039, 2011.

[36] L. Zhang, X.-H. Liu, and Y. Jiang, "Experimental evaluation of a suspended metal ceiling radiant panel with inclined fins," *Energy and Buildings*, vol. 62, no. 7, pp. 522–529, 2013.

[37] Y. Y. Zhu, Q. Zhang, J. P. Liu, and Q. Zhao, "Research on thermal stability of configuration of residential building energy saving exterior wall in Northwestern areas," *Journal of Xi'an University of Technology*, vol. 27, no. 1, pp. 46–50, 2011.

[38] Y. Q. Cui, N. H. Sun, H. B. Cai, and S. M. Li, "Indoor temperature improvement and energy-saving renovations in rural houses of China's cold region—a case study of Shandong Province," *Energies*, vol. 13, no. 4, pp. 1–26, 2020.

[39] S. Gou, Z. Li, Q. Zhao, V. M. Nik, and J.-L. Scartezzini, "Climate responsive strategies of traditional dwellings located in an ancient village in hot summer and cold winter region of China," *Building and Environment*, vol. 86, no. 4, pp. 151–165, 2015.

[40] C. Mitterer, H. M. Künzel, S. Herkel, and A. Holm, "Optimizing energy efficiency and occupant comfort with climate specific design of the building," *Frontiers of Architectural Research*, vol. 1, no. 3, pp. 229–235, 2012.

[41] C. Deng, H. Bai, X. Ma, T. Zhao, S. Gao, and X. Huang, "Spatiotemporal differences in the climatic growing season in the Qinling Mountains of China under the influence of global warming from 1964 to 2015," *Theoretical and Applied Climatology*, vol. 138, no. 3-4, pp. 1899–1911, 2019.

[42] J. Li, X. Feng, J. Yin, and F. Chen, "Change analysis of spring vegetation green-up date in Qinba mountains under the support of spatiotemporal data cube," *Journal of Sensors*, vol. 2020, no. 1, 12 pages, Article ID 6413654, 2020.

[43] Y. Y. Zhu, J. Z. Zhao, G. C. Sang, and Q. Zhao, "Thermal performance and energy-saving construction for rural architecture in Qinba Mountain Areas," *Journal of Ningxia University (Natural Science Edition)*, vol. 38, no. 4, pp. 426–12438, 2017.

[44] C. H. Deng, H. Y. Bai, S. Cao, T. Zhao, and X. P. Ma, "Differences and variations in the elevation-dependent climatic growing season of the northern and southern slopes of the Qinling Mountains of China from 1985-2015," *Theoretical and Applied Climatology*, vol. 137, no. 1-2, pp. 1159–1169, 2018.

[45] Q. Y. Zhang and H. Joe, *Chinese Standard Weather Databank for Buildings*, Machine Industry Press, Beijing, China, 2014.

[46] JGJ/T 267–2012, *Technical Code for Passive Solar Buildings*, China Architecture Building Press, Beijing, China, 2012.

[47] L. Zhao and J. Xu, "Architectural design of residential buildings in Qinba mountains based on knowledge mapping," *Case Studies in Thermal Engineering*, vol. 14, no. 9, pp. 1–7, 2019.

[48] M. M. Yu, Y. Y. Ren, S. H. Liu, and D. M. Ma, "Southern Shanxi Ankang region residence geographic features and its inheritance and development," *Architecture and Culture*, vol. 132, no. 3, pp. 109–111, 2015.

[49] L. W. Dong, "Climate suitability analysis of villages and towns in Southern Shanxi based on climate consultant—taking the Ankang area as an example," *Architecture and Culture*, vol. 180, no. 3, pp. 105-106, 2013.

[50] F. C. Houghtona and C. P. Yaglou, "Determining equal comfort lines," *Journal of the American Society of Heating and Ventilating Engineers*, vol. 29, no. 1, pp. 165–176, 1923.

[51] J. Liu, L. Wang, Y. Yoshino, and Y. Liu, "The thermal mechanism of warm in winter and cool in summer in China traditional vernacular dwellings," *Building and Environment*, vol. 46, no. 8, pp. 1709–1715, 2011.

[52] J. P. Liu and Y. Liu, "Thermal design of a zero energy cave-dwelling solar house," *Acta Energiae Solaris Sinica*, vol. 20, no. 3, pp. 302–310, 1999.

[53] T. Galloway, *Solar House: A Guide for the Solar Designer*, Architectural Press, Paris, England, 2004.

[54] D. A. Mcintyre, *Indoor Climate*, Applied Science Publisher, London, UK, 1980.

[55] ANSI/ASHRAE Standard 55-2013, *Thermal Environmental Conditions for Human Occupancy*, American Society of Heating, Refrigerating and Air conditioning Engineers, Inc., Atlanta, GA, USA, 2013.

[56] P. O. Fanger, *Thermal Comfort*, Danish Technical, Copenhagen, Denmark, 1970.

[57] Q. S. Yan and Q. Z. Zhao, *Building Thermal Process*, China Architecture & Building Press, Beijing, China, 1986.

[58] Y. Z. Li, *Handbook of Thermal Design for Passive Solar House*, Shanghai Scientific & Technical Publishers, Shanghai, China, 1989.

[59] Q. Wang, *Study on Low Energy Consumption Structure System of Qinba Mountainous Building*, Xi'an University of Technology, Xi'an, China, 2018.

[60] GB/T50824-2013, *Design Standard for Energy Efficiency of Rural Residential Buildings*, China Architecture Building Press, Beijing, China, 1993.

[61] 06J607-1, *National Building Standard Design Atlas*, China Planning Press, Beijing, China, 2006.

[62] H. Gao and G. Wei, "Numerical solution of potential problems using radial basis reproducing kernel particle method," *Results in Physics*, vol. 13, no. 2, Article ID 102122, 2019.

[63] H. Gao and G. Wei, "Complex variable meshless manifold method for transient heat conduction problems," *International Journal of Applied Mechanics*, vol. 9, no. 5, pp. 1–20, Article ID 1750067, 2017.

[64] Z. J. Meng, H. Cheng, L. D. Ma et al., "The dimension splitting element-free Galerkin method for 3D transient heat conduction problems," *Physics, Mechanics & Astronomy*, vol. 62, no. 4, pp. 1–12, Article ID 040711, 2019.

[65] J.-F. Wang and Y.-M. Cheng, "A new complex variable meshless method for transient heat conduction problems," *Chinese Physics B*, vol. 21, no. 12, pp. 1–9, Article ID 120206, 2012.

[66] G. Zhang, F. Zhang, and H. Ren, "Accuracy analysis of interpolating element-free galerkin (IEFG) method in solving transient heat conduction problems," *International Journal of Applied Mechanics*, vol. 8, no. 6, pp. 1–18, Article ID 1650078, 2016.

[67] M. J. Peng and Y. M. Cheng, "A boundary element-free Galerkin (IEFG) for two-dimensional potential problems," *Engineering Analysis with Boundary Elements*, vol. 36, no. 5, pp. 77–82, 2009.

[68] S. Mukherjee and Y. Liu, "The Boundary element method," *International Journal of Computational Methods*, vol. 10, no. 6, pp. 1–91, Article ID 1350037, 2013.

[69] Z. Q. Zhang, Z. J. Wang, and L. M. Lian, "Numercal SsimuIation for indoor thermal environment in residential buildings," *Building Energy and Environment*, vol. 23, no. 6, pp. 88–92, 2004.

[70] K. Matsunawa, H. Iizuka, and S. Tanabe, "Development and application of an underfloor air-conditioning system with improved outlets for a 'smart' building in Tokyo," *Ashrae Transactions*, vol. 101, no. 1, pp. 887–901, 1995.

[71] GB 50176-2016, *Code for Thermal Design of Civil Building*, China Architecture Building Press, Beijing, China, 2016.